APPLIED PHYSICS

Emergent hydrodynamic bound states between magnetically powered micropropellers

Fernando Martinez-Pedrero,[1,2] Eloy Navarro-Argemí,[1,3] Antonio Ortiz-Ambriz,[1,5] Ignacio Pagonabarraga,[1,3,4] Pietro Tierno[1,3,5]*

Hydrodynamic interactions (HIs), namely, solvent-mediated long-range interactions between dispersed particles, play a crucial role in the assembly and dynamics of many active systems, from swimming bacteria to swarms of propelling microrobots. We experimentally demonstrate the emergence of long-living hydrodynamic bound states between model microswimmers at low Reynolds numbers. A rotating magnetic field forces colloidal hematite microparticles to translate at a constant and frequency-tunable speed close to a bounding plane in a viscous fluid. At high driving frequency, HIs dominate over magnetic dipolar ones, and close propelling particles couple into bound states by adjusting their translational speed to optimize the transport of the pair. The physical system is described by considering the HIs with the boundary surface and the effect of gravity, providing an excellent agreement with the experimental data for all the range of parameters explored. Moreover, we show that in dense suspensions, these bound states can be extended to one-dimensional arrays of particles assembled by the sole HIs. Our results manifest the importance of the boundary surface in the interaction and dynamics of confined propelling microswimmers.

INTRODUCTION

Active particles moving in viscous fluids and propelled by external fields (*1*–*5*) or chemical reactions (*6*, *7*) represent a rich and growing area of research, where many emergent nonequilibrium phenomena can be observed (*8*). The dynamics of an ensemble of active particles are governed by the interplay between propulsion, thermal noise, and pair interactions coupled with the dispersing medium. External fields usually induce alignment and fast assembly of the particles due to dipolar forces (*9*). A subtler role is played by hydrodynamic interactions (HIs) (that is, the solvent-mediated long-range interactions) that can be excited by the random or directed motion of the particles in the fluid medium. These interactions depend on the particle speed and angular velocities, because the solvent couples to the particles through forces and torques. Thus, HIs cannot be described by a simple potential term, in contrast to dipolar forces.

Colloidal dispersions constitute a suitable model system to study the complex effects of HIs at low Reynolds numbers, given the ability to manipulate (*10*, *11*), align (*12*, *13*), or rotate (*14*, *15*) the particles with external fields. More generally, HIs are not only limited to colloids but also affect the dynamics of many complex and biological systems (*16*). Examples span from the spontaneous formation of cell vortex arrays (*17*) to synchronized cilia beating (*18*) and the attraction and dancing of a pair of Volvox algae (*19*). Thus, understanding the effect of HIs in interacting microscale objects is crucial in both applied and fundamental research.

When the motion of the propelled particles is affected by a nearby wall, the confinement may have a strong influence on the system dynamics. For example, the proximity of a surface explains the circular path of motile *Escherichia coli* (*20*), explains the attraction of model swimmers toward the surface (*21*), or can be even used to steer the particles along defined paths (*22*–*24*). Most of the experiments based on trapped or driven colloidal particles used as model system for hydrodynamic coupling have been mainly focused on the direct interactions between the couple without exploring the effect of a confining plane on the collective dynamics.

Here, we investigate the interactions between a pair of model microswimmers composed of monodisperse ferromagnetic hematite microparticles driven above a plane by an external rotating magnetic field. At high driving frequencies, the spinning particles generate large hydrodynamic flow fields, and the corresponding HIs dominate over the magnetic ones, giving rise to different dynamic states. We report the direct experimental observation of hydrodynamic bound states with a long lifetime, where two close propelling particles adjust their velocities to couple their trajectory. Depending on the relative position of the particles, the bound colloids could either translate tip to tip or speed up by aligning such that the relative position is perpendicular to the particles' long axes. The experiments are complemented with a theoretical model that takes into account the presence of the bounding plane, allowing to capture the essential physics of the process.

RESULTS

In our experiments, we use "peanut"-shaped hematite microparticles, characterized by a long (short) axis equal to $a = 2.5$ μm ($b = 1.4$ μm) (see Fig. 1, A and B). After dilution in highly deionized water, the particles sediment due to a density mismatch above a glass substrate, where they display small Brownian motion with negligible out-of-plane fluctuations. The particles have a homogeneous mass distribution (*25*) and present a small permanent moment $\boldsymbol{m}$ perpendicular to their long axis (see Materials and Methods). We determine the amplitude of the particle moment by following the orientational angle θ of individual particles when subjected to a static magnetic field $\boldsymbol{H}$. Figure 1C shows the evolution with time of θ for five different particles and the corresponding fits to the experimental data (see Materials and Methods). From these fits, we find a distribution of moments $P(m)$ centered at $\langle m \rangle = 9 \cdot 10^{-16}$ A m^2 and having a Gaussian-like shape with a variance $\sigma_m = 3 \cdot 10^{-16}$ A m^2.

We spin the hematite particles by applying a rotating magnetic field circularly polarized in the $(\hat{x}, \hat{z})$ plane, $\boldsymbol{H}(t) = H_0(\cos(\omega t)e_x - \sin(\omega t)e_z)$

[1]Departament de Física de la Matèria Condensada, Universitat de Barcelona, Barcelona, Spain. [2]Departamento de Química Física I, Universidad Complutense de Madrid, Madrid, Spain. [3]Universitat de Barcelona Institute of Complex Systems, Barcelona, Spain. [4]Centre Européen de Calcul Atomique et Moléculaire, École Polytechnique Fédérale de Lausanne, Batochime, Avenue Forel 2, 1015 Lausanne, Switzerland. [5]Institut de Nanociència i Nanotecnologia, Universitat de Barcelona, Barcelona, Spain.
*Corresponding author. Email: ptierno@ub.edu.

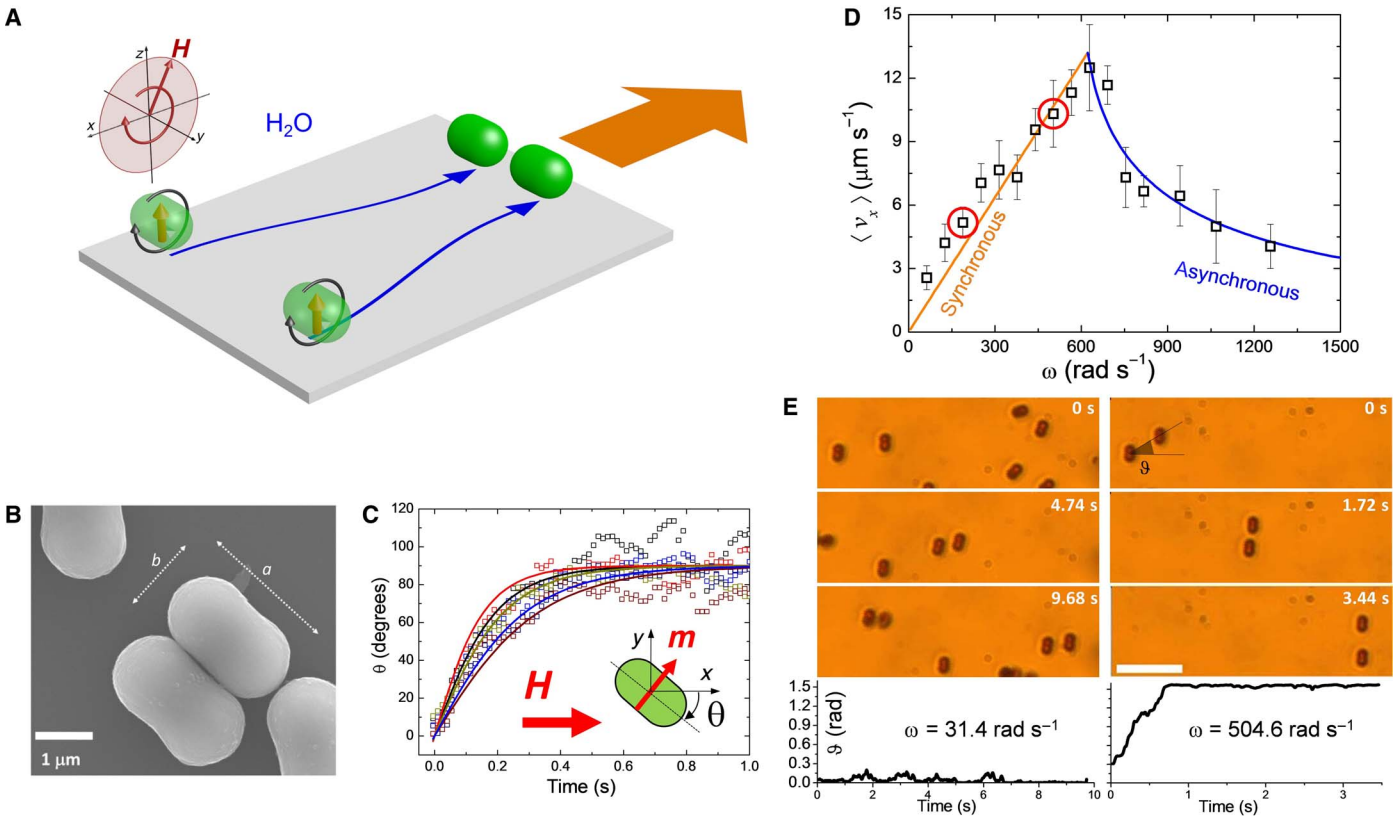

Fig. 1. Propulsion of the hematite micropropellers. (**A**) Schematic showing two hematite particles subjected to a rotating magnetic field circularly polarized in the (*x*, *z*) plane. (**B**) Scanning electron microscope image of the hematite particles, where *a* and *b* are the long and short axes, respectively. (**C**) Orientational angle θ between the particle long axis and an applied field ***H***. The particle moment is obtained by balancing the magnetic and viscous torque during reorientation (see Materials and Methods). (**D**) Average speed $\langle v_x \rangle$ versus driving frequency ω of one micropropeller subjected to a rotating field with amplitude of H_0 = 4400 A m^{-1}. Orange and blue fits denote synchronous and asynchronous regimes. (**E**) Microscope images showing a pair of propelling particles at frequencies ω = 188.5 rad s^{-1} (left) and ω = 502.6 rad s^{-1} (right). Scale bar, 10 μm. (see movie S1). Bottom: The evolution with time of the relative positional angle θ.

with angular frequency ω and amplitude H_0 (Fig. 1A). The applied modulation induces a magnetic torque $\boldsymbol{T}_m = \mu_0 \boldsymbol{m} \times \boldsymbol{H}$, which produces a particle rotation close to the substrate at an average angular velocity $\langle \Omega \rangle$, with $\mu_0 = 4\pi \cdot 10^{-7} H\ m^{-1}$. The solid surface breaks the spatial symmetry, and the anisotropic particles roll close to the plane due to the rotation-translation hydrodynamic coupling (*26*). The net drift velocity is a function of the angular speed, $\langle v_x \rangle = b f_r \langle \Omega \rangle / 2$, being f_r a small correction factor resulting from the wall proximity. This value can be calculated by assuming that the translational motion of the ellipsoids is due to the sole rotation induced by the magnetic field. In particular, $f_r = f_{rot}/f_{tran}$, being $f_{rot} = \frac{2}{15} \log \frac{b}{2h} - 0.2526$ and $f_{tran} = \left(\frac{8}{15} + \frac{32}{375}\frac{h}{b}\right)\left(\log \frac{b}{h} + 0.2526\right)$, as derived in the lubrication limit and for a small distance *h* between the wall and the surface of a particle of radius *b*/2 (*26*). We estimate the average elevation of the particle center from the surface as *h* = 1.0 μm using the orange fit in Fig. 1D. Below a critical frequency ω_c, single particles follow the field rotation synchronously, with $\langle \Omega \rangle = \omega$. For $\omega > \omega_c$, the particles follow the driving magnetic field asynchronously, and the $\langle v_x \rangle$ decreases as the ω increases. Neglecting thermal fluctuations, the average rotational speed follows $\langle \Omega \rangle = \omega\left(1 - \sqrt{(1 - (\omega_c/\omega)^2)}\right)$ (*27*), as shown by the blue fit in Fig. 1D. Note that the hematite particles display a weak magnetic-moment polydispersity, as also measured in Fig. 1C. As a consequence, when close to ω_c, the propellers show a speed distribution $P(\langle v_x \rangle)$, and similar particles may display different average speeds being in the synchronous or asynchronous regime.

When we increase the density of the colloidal system, close particles start to interact due to magnetic and viscous forces. The driving field aligns the permanent moments of the micropropellers, ensuring that the particles always roll perpendicular to their long axis. Thus, only the angle ϑ between $\hat{x}$ axis and the line connecting the center of the two particles is needed to describe the relative orientation of the pair (Fig. 1E). To classify the type of dynamic states observed, we vary mainly the driving frequency that controls the average speed and fix the field amplitude. We find that the relative arrangements of pairs of particles strongly depend on their rotational motion. At low driving frequencies ($\omega \lesssim 300$ rad s^{-1}), the propellers tend to arrange such that the relative position is perpendicular to the particles' long axes to minimize the magnetic energy of the couple (first column of Fig. 1E). By contrast, we find that at high driving frequencies ($\omega \gtrsim 400$ rad s^{-1}), the fast spinning of the particles induces strong HIs, and the propellers assemble forming a different bound state, in which the particles align along their long axis during propulsion (second column in Fig. 1E), even if dipolar interactions are repulsive in this configuration, as demonstrated in the next section.

We can identify the emergence of these bound states by measuring the order parameter $\alpha = (v_{rel}/v_{cv})^2$, based on the speed $v_{1,2}$ of the particles, which quantifies the ratio between the relative velocity $v_{rel} = v_1 - v_2$

and center of velocity $v_{cv} = (v_1 + v_2)/2$ of the couple. Figure 2 (A to C) shows three representative cases illustrating the behavior of a couple of propellers with the low-frequency situation displayed in the first column. At high frequencies, we find that colloidal pairs tend to either align at a finite angle ($\vartheta \in [\pi/6, \pi/3]$) [second column in Fig. 2 (A to C)] or arrange themselves parallel to each other such that $\vartheta = \pi/2$ [third column in Fig. 2 (A to C)]. In the last two cases, the two particles form a transient hydrodynamic state that can last more than 6 s and where the two particles adjust their velocities such that v_{cv} either increases ($\vartheta \to 0$) or decreases ($\vartheta \to \pi/2$), and v_{rel} almost vanishes. We quantify the duration of these bound states by measuring the histogram of the distribution of time lapses during which $\alpha < 0.01$. This threshold value arises from the observed polydispersity of the particle velocity close to the critical frequency. For a pair of propellers whose angular velocities differ by 10 %, one has $\alpha \sim (d\omega/\omega)^2 = 0.01$, with $d\omega = 0.1\omega$. We find that with this choice, these states have a longer duration at high frequencies, even if magnetic interactions oppose their development, as shown by Fig. 2 (D and E). The origin of the finite lifetime of these bound states may be due to thermal noise or disorder in the experimental system. This disorder may arise from small polydispersity in the particle shape or magnetic moments or from fluctuations in the particle elevation during propulsion that may induce changes of the hydrodynamic lift forces. These changes may favor direct or soft collisions between the particles and the wall, thus constituting an additional source of noise. However, we have found cases where the bound states were observed along the whole sample area, providing a strong indication that the observed trajectories do not correspond to simple scattering events between the particles.

Self-organization induced by HIs at low Reynolds number is attracting remarkable interest due to its direct connection with assembly and swarming in active living systems (*28*–*32*). We demonstrate that our colloidal propellers, when driven at high frequencies, can be organized into metastable, elongated structures maintained only by HIs. Figure 3A shows a series of images illustrating the assembly process of a chain composed of five hydrodynamically coupled propellers driven by the rotating field. As shown in movie S3, to assemble this structure and avoid the travelling of particles outside the field of view, the propellers were driven first forward and later backward when reaching the limit of the observation area. This change of direction was obtained by switching the x component of the applied field, $H_x = -H_x$. Reversing the field does not disentangle the formed bound state because gravity and disorder break the symmetry under time inversion at low Reynolds numbers. From the particle positions, we determine the angle ϑ and the velocities $\langle v_{cv} \rangle$ and $\langle v_{rel} \rangle$, which are now averaged over all pairs of particles within the assembly. As shown in Fig. 3B, after a transient regime, all quantities stabilize to a stationary value where the relative speed between the composing particles approaches zero. The composite chain is rather stable, propelling as a compact rod with a center of velocity $\langle v_{cv} \rangle \sim 10\ \mu m\ s^{-1}$.

THEORETICAL MODEL

Hydrodynamic interactions

We model the propelling couple as a pair of rotating solid spheres above a wall. The solid surface can be accounted through an hydrodynamic singularity placed at the same distance below the position of the interface, namely, a particle rotating in the opposite sense, plus additional stresslet and source doublets (*33*). We assume that the applied field forces the particles to rotate at a given angular velocity, which may differ from the driving frequency depending on the nature of each colloidal particle. Thus, the flow $\boldsymbol{u}$ generated by a colloid of radius a and rotating at a prescribed angular velocity Ω can be estimated by considering a rotlet located at a distance h from the wall, as developed in the study of Blake and Chwang (*33*) using the Blake tensor

$$\frac{u_i}{a^3} = \frac{\epsilon_{ijk}\Omega_j r_k}{|r|^3} - \frac{\epsilon_{ijk}\Omega_j R_k}{|R|^3} + 2h\epsilon_{kjz}\Omega_j\left(\frac{\delta_{ik}}{|R|^3} - \frac{3R_iR_k}{|R|^5}\right) + 6\epsilon_{kjz}\frac{\Omega_j R_i R_k R_z}{|R|^5} \quad (1)$$

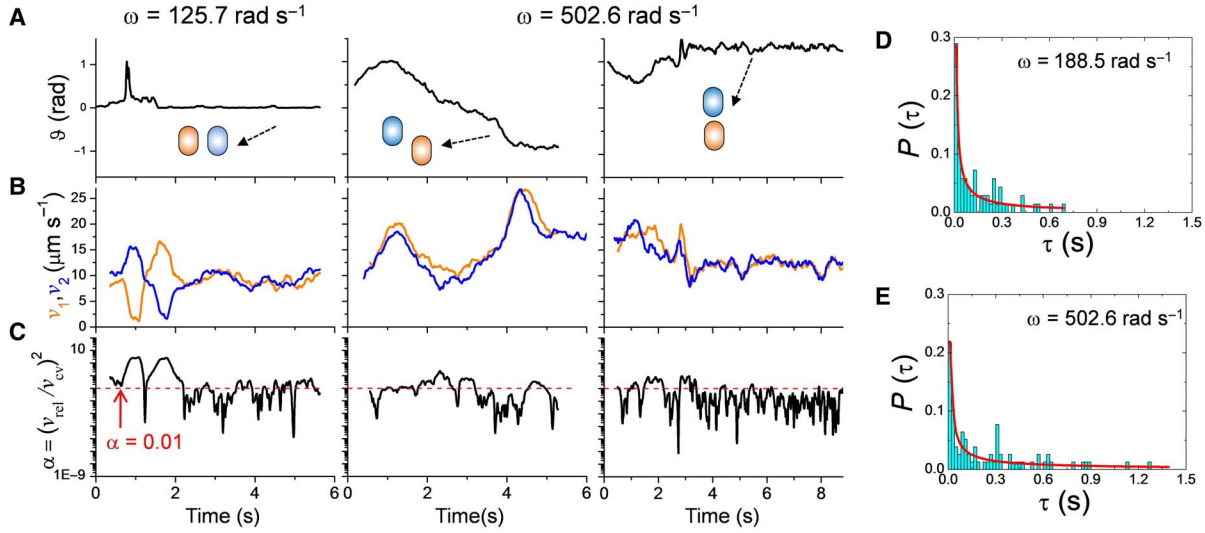

Fig. 2. Observation of the bound states. (**A** to **C**) Sequence of graphs illustrating (A) the time evolution of the angle ϑ, (B) particle velocities v_1, v_2, and (C) normalized relative velocity squared $\alpha = (v_{rel}/v_{cv})^2$ for a pair of propellers driven by a rotating field with amplitude of $H_0 = 4400$ A m^{-1} and at two different frequencies. The first column refers to $\omega = 125.7$ rad s^{-1} and second and third columns to $\omega = 502.6$ rad s^{-1}. The increase in speed of the pair of propellers is shown in movie S2. The time $t = 0$ corresponds to an arbitrary starting point. (**D** and **E**) Probabilities $P(\tau)$ of lifetimes τ, where the pair of propellers have $\alpha < 0.01$ for frequencies $\omega = 125.7$ rad s^{-1} (D) and $\omega = 502.6$ rad s^{-1} (E). The continuous red lines are fits to the data of an algebraic function as a guide to the eye.

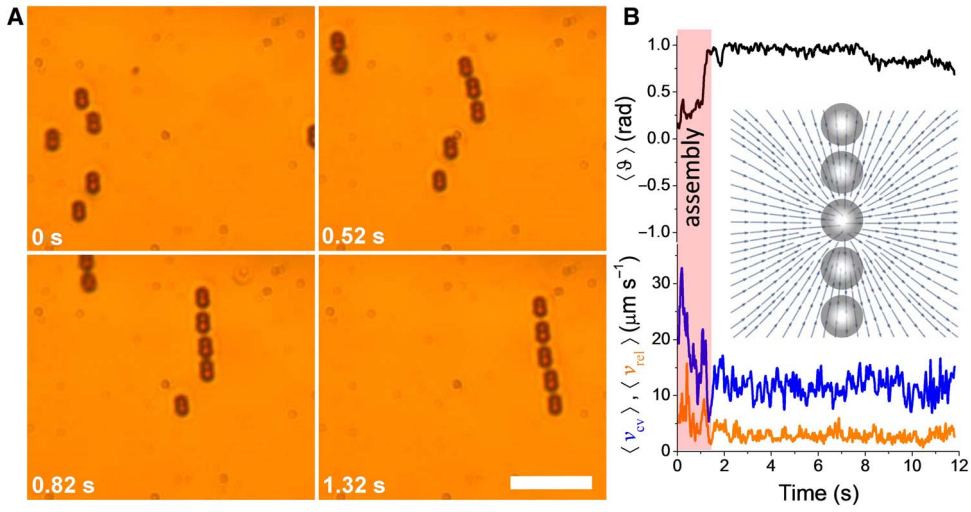

Fig. 3. Self-assembly due to sole HI. (**A**) Sequence of images showing the formation of a chain of five propellers under a rotating field with amplitude of $H_0 = 4400$ A m^{-1} and frequency of $\omega = 502.6$ rad s^{-1}. Scale bar, 10 μm. The time $t = 0$ corresponds to an arbitrary staring point. The corresponding video is movie S3. (**B**) Evolution with time of the average positional angle ϑ (top), $\langle v_{cv} \rangle$ in blue and $\langle v_{rel} \rangle$ in orange (bottom). The shaded red region in the graph denotes the assembly stage. Inset illustrates the flow velocity u_x calculated at the same elevation of a chain composed of five propellers.

Here, $\boldsymbol{r}$ is the position vector from the center of the particle, $\boldsymbol{R}$ is the position of its image, and ϵ_{kjz} is the Levi-Civita tensor. From Eq. 1, we derive analytic expressions for the speeds $\boldsymbol{v}_{1,2}$ for two spheres 1, 2 rotating with angular speed $\Omega_{1,2}$ and at an elevation of $h_{1,2}$. The complete set of equations resulting from Eq. 1 is given in the Supplementary Materials.

From the model, we can first resolve the complex dynamics of the particles in a bound state. Typical trajectories of the center of velocities of the two particles forming a pair are shown in Fig. 4 (A and B) and can be compared to movie S4, when driven by an external rotating field in the synchronous regime. When the particles form the bound state, their relative distance is not fixed in one period, but the two propellers perform a periodic motion around each other in the three-dimensional (3D) space. During this motion, the particle elevation and their relative distance vary periodically with time (Fig. 4, A and B). Moreover, we find that depending on the initial angle and distances, the pair may form different types of cyclic states, all of them characterized by a relative rotation of one colloid with respect to the other. This situation occurs when gravitational forces are negligible, as shown in Fig. 4A. In the presence of gravity, the bound orbits become almost independent from its initial conditions, and the pair of ellipsoids has negligible oscillation along the z direction, as shown in Fig. 4B. The relative motion between the two particles can be visualized from simulations for the case $F_g = 0$, while being more difficult to be quantified from the experiments.

Role of gravity in the bound state

We also consider the effect of gravity on the dynamics of the pair of particles. The gravitational force $F_g = \Delta\rho g V$ is balanced by the repulsive electrostatic interaction $F_{el} = \frac{A}{\lambda} e^{-z/\lambda}$ arising from the charge of the particle and the bounding plate. Here, $V = (4/3)\pi a^3$ is the particle volume, $\Delta\rho = 4.25$ g cm^{-3} is the density mismatch between the particle ($\rho_p = 5.25$ g cm^{-3}) and the suspending medium ($\rho_w = 1$ g cm^{-3}), A is a prefactor that depends on the surface charge density, and λ is the Debye screening length. For small displacement $z = h + \delta$, near the equilibrium elevation of the particle h, one can derive an effective elastic force with a coupling constant given by, $K = \frac{gV\Delta\rho}{\lambda}$. We consider the effect of the vertical forces as a stokeslet and add its contribution to eq. S1, where the resulting set of equations is given. These equations allow testing for the role of gravity in the bound state by varying the gravitational force $F_g = \Delta\rho g V$. In Fig. 4C, we plot the mean distance between two particles in a bound state as a function of the period of the rotating magnetic field. The different curves refer to situations where we vary the ratio $F_{g/h}$ between F_g and the viscous force $F_h = 3\pi\eta\Omega a^2/4$, where $\eta = 10^{-3}$ Pa · s is the solvent viscosity and we used $h \sim a$ as the particle elevation from the substrate. In all cases, we find that for small initial distance between the particles, stable bound states can be formed regardless of gravity. Thus, we still observe the formation of these states and find that the main effect of gravity is that it reduces the oscillations of the particle elevations when they couple. The consequence of this constrained motion is that the relative positional angle between the particles changes, as shown in Fig. 4D. Starting from a configuration of $\vartheta = 45^\circ$, even small gravitational forces ($F_{g/h} \sim 10^{-2}$) can stabilize the couple of particles in the tip-to-tip configuration, as illustrated in the second column of Fig. 1E. This configuration is linearly unstable for the purely hydrodynamic model, but it becomes stable in presence of gravity.

Magnetic interactions

Here, we show that the dipolar interactions between a pair of propellers are effectively attractive (repulsive) when their relative position is perpendicular (parallel) to the particle long axis. The magnetic dipolar interactions between a pair of particles, (i, j), with moments $\boldsymbol{m}_i, \boldsymbol{m}_j$ and at a distance $\boldsymbol{r}_{ij} = |\boldsymbol{r}_i - \boldsymbol{r}_j|$, are given by $U_d = \frac{\mu_0}{4\pi}\left(\frac{m_i m_j}{r_{ij}^3} - \frac{3(m_i \cdot r_{ij})(m_j \cdot r_{ij})}{r_{ij}^5}\right)$. Thus U_d is maximally attractive (repulsive) for particles with magnetic moments parallel (perpendicular) to $\boldsymbol{r}_{ij}$. If we consider two particles confined on the $(\hat{x}, \hat{y})$ plane and with the dipole moments aligned with a magnetic field rotating in a perpendicular $(\hat{x}, \hat{z})$ plane, as shown in Fig. 1A, then we can calculate the average interaction energy between them by performing a time average (*9*). We find that the effective potential is attractive, $\langle U_d \rangle = -\frac{\mu_0 m^2}{8\pi(x+z)^3}$, leading to chaining in the $(\hat{x}, \hat{z})$ plane, while being repulsive along the perpendicular $\hat{y}$ direction, $\langle U_d \rangle = \frac{\mu_0 m^2}{4\pi y^3}$.

Further, we can put forward a simple argument to explain the different arrangements from the changes in magnitude of the competing

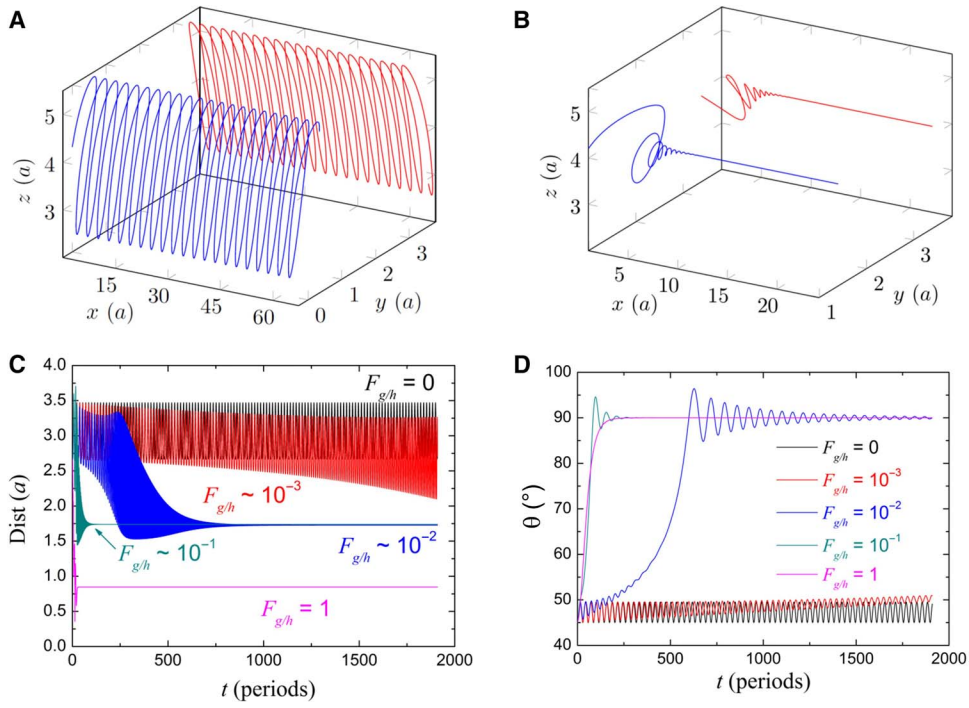

Fig. 4. Hydrodynamic bound states. (**A** and **B**) 3D trajectories of two particles (one in blue and the other in red) in a hydrodynamic bound state. The data are obtained from numerical simulations of the equations in the Supplementary Materials, with an initial angle $\vartheta = 45°$, a distance of $d = 2.67a$, being a the particle radius for $F_{g/h} = 0$ (A) and $F_{g/h} = 10^{-1}$ (B). $F_{g/h}$ denotes the ratio between the gravitational F_g and vicous F_h forces (see movie S4). (**C** and **D**) Distance (C) and angle (D) between the two particles measured in term of the particle radius a versus period of the driving field for different values of $F_{g/h}$.

forces acting on the pair. The attractive force between two equal dipoles m at distance $r = 2a$ is given by $F_m = 3\mu_0 m^2/(64\pi a^4)$, whereas the viscous force generated by a single propeller is $F_h = 3\pi\eta\Omega a^2/4$, where $h \sim a$. Hence, for $m = 9 \cdot 10^{-16}$ A m^2 and $a = b/2 = 0.7$ μm, we find that $F_h/F_m = 16\pi^2\eta\Omega a^6/(\mu_0 m^2) = 0.02$ Ω. Thus $F_h = 0.6F_m$ for $\Omega = 31.4$ rad s^{-1}, whereas $F_h = 9.1F_m$ for $\Omega = 504.6$ rad s^{-1} Finally, note that the magnetic interactions due to the permanent moments of the particles are relatively small, and the tip-to-tip (side-by-side) alignment corresponds to an interaction potential $U_d = 7.3\ k_B T$ ($U_d = 1.3\ k_B T$), that is, much lower than the interactions resulting from induced dipoles (*27*). Thus, although in our previous works (*27*) the magnetic interactions were essential to maintain the propelling structures, here, the dynamic states observed at large frequencies are bound purely by HIs mediated through the confinement.

DISCUSSION

We test the model by measuring the average translational speed $\langle v_{cv}\rangle$ of a pair of particles in a bound state. In particular, we decompose this velocity in two components parallel ($\langle v_{cv}\rangle \cdot \hat{x}$) and perpendicular ($\langle v_{cv}\rangle \cdot \hat{y}$) to the propulsion direction ($\hat{x}$ axis) imposed by the rotating field. Both quantities, normalized with respect to the speed of a single propeller $\langle v_0\rangle$, are plotted versus the positional angle ϑ in Fig. 5 (A and B) and at different center-to-center distances r. The image shows the comparison between the experimental data (symbols) and the analytical results (continuous line), which were plotted assuming that both particles have the same elevation, $h \sim 1$ μm, as determined from the fits in Fig. 1D, and are driven in the synchronous regime with $\Omega_{1,2} = \omega = 502.6$ rad s^{-1}. The data and the fits show that along the propulsion direction, the pair of particles decreases the average speed with the angle ϑ. Thus, the highest speed is measured in the configuration where two particles have their long axes placed side by side, as shown in the first column of Fig. 2. The behavior of the perpendicular component also illustrates the tendency of the pair to have a higher transversal velocity at intermediate angles, in agreement with the experimental observation where pairs of propellers were found to speed up when placed at $\vartheta \sim 45°$ (see also Fig. 2B, second row). Despite the approximations used in the model, which considers the magnetic propellers as point particles rather than extended objects with a complex, peanut-like shape (Fig. 1B), we obtain a quantitative agreement between the theoretical predictions and the experimental data. This agreement confirms that the model can capture the physical mechanisms that induce these bound states. The strong alignment induced by the applied field prevents any in-plane rotational motion of the propelling particles, reducing the effect of the anisotropic shape on their dynamics. The small deviations of the theoretical curves from the experimental data observed at low distances between the particles may be effectively attributed to the extended shape of the propellers. These deviations can be corrected by considering a more refined account of the hydrodynamically induced flows, a subject for future theoretical works.

From Eq. 1, it is also possible to calculate the net flow field velocity generated by the assembly, which is presented in the small inset in Fig. 3B as a streamplot graph. The chain of propellers generates a net flux toward the direction of motion, perpendicular to the chain long axis and focused toward the center of the assembly. This flow field may be used to manipulate unbound nonmagnetic objects in a fluid, both pulling and pushing them by varying the propulsion direction of the chain through the sense of rotation of the actuating magnetic field. Plans to explore these exciting possibilities are underway.

We next comment on the general implications of our findings for other active/biological systems. The presence of boundaries or confinement has

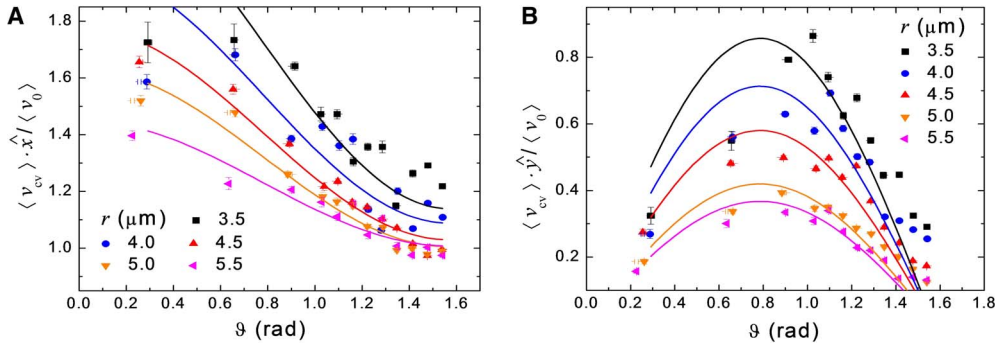

Fig. 5. Average center of velocity of the pair. (**A** and **B**) Components of the velocity $\langle v_{cv} \rangle$ along the $\hat{x}$ (A) and $\hat{y}$ (B) directions versus angle ϑ. The pair of propellers forming the bound states is driven by a rotating field with amplitude $H_0 = 4400$ A m^{-1} and frequency $\omega = 502.6$ rad s^{-1}. $\langle v_0 \rangle = 10.3$ μm s^{-1} denotes the speed of a single propeller driven by the same field. r is the center-to-center distance. Scattered symbols denote experimental data; continuous lines are fits following the model developed in the text.

an important impact on the propulsion and dynamics of several biological systems at the microscale. Boundaries modify the hydrodynamic stresses acting on self-propelling particles, and because of that, these particles may change their speed, trajectories, and orientations, or even reduce their interactions, see study of Lauga and Powers (*16*) for a comprehensive review. Here, we have demonstrated that a simple system composed of a pair of magnetically driven propellers displays attractive HIs during motion in presence of a boundary. Whereas at the single-particle level our driven system differs from a self-propelling one, the latter being characterized by a given randomness in its trajectory, at a finite volume fraction, long-range interactions mediated by the dispersing fluid arise in both cases. These interactions lead to dispersion, which plays a role similar to the noise. Therefore, these interactions, together with the irregularities in the colloidal and bounding surfaces, provide sources of noise that render the motion of the driven system effectively analogous to an active system. Our finding may be also applied to understand the self-organization of microswimmers close to a surface, when these swimmers are characterized by a small rotational diffusion and thus more persistent trajectories. Further examples not only include the dynamics of sperm cells (*34*) and the bound states formed by algae (*19*) but also the assembly of field driven propellers near a surface (*35*). Apart from self-propelling systems, the hydrodynamically bound chains of magnetic propellers have also a direct connection with the alignment of colloidal particles under shear flow. Theoretical studies have investigated the emergence of 1D string structures of hard-sphere colloids by using a shear flow (*36*, *37*). In particular, it was predicted that sheared particles could organize either in strings along the direction of motion (flow alignment) or perpendicular to it (vorticity alignment). The latter and most counterintuitive case was, only recently, experimentally demonstrated via confocal microscopy of hard-sphere silica particles (*38*). Although our propellers interact magnetically, the strong hydrodynamic coupling between them can organize these particles into elongated chains that grow perpendicular to their propulsion direction. The analogy with the previous work arises from the fact that propulsion close to a plane acts as an effective shear to the colloidal system. Thus, our work represents an alternative demonstration with a non–hard-sphere system of this counterintuitive phenomenon at the microscale.

In conclusion, we have investigated the long-range HIs between two model microswimmers composed of magnetically propelled anisotropic hematite particles. When HIs dominate over the dipolar one, we observe the emergence of cooperative states that are hydrodynamically bound, where the particles adjust their speed by slowing down or speeding up due to the generated flow field. Our findings may help understand similar cooperative mechanisms occurring in confined biological systems at low Reynolds numbers and could be a starting point toward the description of the dynamics in dense-driven particle suspensions.

MATERIALS AND METHODS

Magnetic propellers and experimental setup

Ellipsoidal hematite (γ-Fe_2O_3) particles were synthesized by following the "gel-sol" technique (*25*). Specifically, we gradually added to an iron chloride hexahydrate solution (54.00 g $FeCl_3 - 6H_2O$ in 100 ml of highly deionized water) a sodium hydroxide solution (19.48 g of NaOH in 90 ml of water) and stirred both solutions at 75°C. After 5 min, we added 10 ml of an aqueous solution containing 0.29 g of potassium sulfate (K_2SO_4) to the stirring mixture. The resulting brown mixture was then stirred for another 5 min, hermetically sealed, and aged in an oven at 100°C for 8 days.

The ellipsoidal-like particles were then recovered by diluting the suspension with highly deionized water, letting the particles sediment and removing the resulting yellowish brown supernatant, a procedure that was repeated several times. To avoid sticking of the particles to the glass substrate, we then functionalized the hematite ellipsoids with SDS.

The measurement cell was placed in the center of two orthogonal pairs of coils arranged on the stage of an optical microscope and aligned along the x and z axes. To apply a rotating field in a plane, we connected the coils with a wave generator (TGA1244, TTi) feeding a power amplifier (AMP-1800, AKIYAMA or BOP 20-10M, Kepco), and two sinusoidal currents with 90° phase shift were passed through the coils. The particle dynamics were recorded by using a charge-coupled device camera (Basler Scout scA640-74fc) working at 75 frames per second. The camera was mounted on top of a light microscope (Eclipse Ni, Nikon) equipped with different magnification objectives (100, × and 40 ×) and a 0.45 × television lens adapter. The positions of the particles were obtained from the analysis of .AVI videos recorded via a commercial software (StreamPix, NorPix).

Determination of the magnetic moments

The perpendicular magnetic moment in the particles resulted from the structure of hematite that crystallized in the corundum form, where the Fe cations were antiferromagnetically aligned along the c axis (*25*). Above the Morin temperature ($T_m \sim 263$ K), the hematite became weakly ferromagnetic, and the magnetic spins were mostly aligned in the basal

plane, thus perpendicular to the particle long axis. We measured the distribution of magnetic moments by following the orientation of different hematite particles subjected to an external static magnetic field $\boldsymbol{H}$, as shown in the schematic in Fig. 1C. In the first approximation, we assumed that the shape of our hematite particle resembled that of an ellipsoid and thus used the friction coefficient of ellipsoid in water to describe the particle dynamics. When reoriented by the external field, the magnetic torque acting on the ellipsoid, $\tau_m = \mu_0 \boldsymbol{m} \times \boldsymbol{H}$, was balanced by the viscous torque arising from its rotation in the fluid, $\tau_v = -\xi_r \dot{\theta}$. Here, $\mu_0 = 4\pi \cdot 10^{-7}$H m^{-1} and ξ_r are the rotational friction coefficient of the ellipsoid. By solving the torque balance equation, $\tau_m + \tau_v = 0$, and taking into account that the angle between the permanent moment and the ellipsoid long axis is $\pi/2$, we arrived at the equation

$$\theta(t) = 2\tan^{-1}\left[\tanh\left(\frac{t}{\tau_r}\right)\right] \quad (2)$$

with $\tau_r = 2\xi_r/(\mu_0 mH)$ as the relaxation time. The rotational friction coefficient for a prolate ellipsoid rotating around its short axis can be written as $\xi_r = 8\pi\eta V_c f_r'$, where $V_c = (4\pi ab^2)/3$ is the volume of the ellipsoid, and f_r' is a small geometrical factor, which depends on the lengths of the ellipsoid long and short axes (*26*).

SUPPLEMENTARY MATERIALS

Supplementary material for this article is available at http://advances.sciencemag.org/cgi/content/full/4/1/eaap9379/DC1

Theoretical Model

movie S1. Movie corresponding to Fig. 1E.

movie S2. Movie corresponding to Fig. 2B.

movie S3. Movie corresponding to Fig. 3A.

movie S4. Movie corresponding to Fig. 4A.

REFERENCES AND NOTES

1. R. Dreyfus, J. Baudry, M. L. Roper, M. Fermigier, H. A. Stone, J. Bibette, Microscopic artificial swimmers. *Nature* **437**, 862–865 (2005).
2. P. Tierno, R. Golestanian, I. Pagonabarraga, F. Sagués, Controlled swimming in confined fluids of magnetically actuated colloidal rotors. *Phys. Rev. Lett.* **101**, 218304 (2008).
3. A. Snezhko, M. Belkin, I. S. Aranson, W.-K. Kwok, Self-assembled magnetic surface swimmers. *Phys. Rev. Lett.* **102**, 118103 (2009).
4. L. Zhang, J. J. Abbott, L. Dong, K. E. Peyer, B. E. Kratochvil, H. Zhang, C. Bergeles, B. J. Nelson, Characterizing the swimming properties of artificial bacterial flagella. *Nano Lett.* **9**, 3663–3667 (2009).
5. A. Bricard, J.-B. Caussin, N. Desreumaux, O. Dauchot, D. Bartolo, Emergence of macroscopic directed motion in populations of motile colloids. *Nature* **503**, 95–98 (2013).
6. W. F. Paxton, K. C. Kistler, C. C. Olmeda, A. Sen, S. K. St. Angelo, Y. Cao, T. E. Mallouk, P. E. Lammert, V. H. Crespi, Catalytic nanomotors: Autonomous movement of striped nanorods. *J. Am. Chem. Soc.* **126**, 13424–13431 (2004).
7. J. R. Howse, R. A. L. Jones, A. J. Ryan, T. Gough, R. Vafabakhsh, R. Golestanian, Self-motile colloidal particles: From directed propulsion to random walk. *Phys. Rev. Lett.* **99**, 048102 (2007).
8. I. S. Aronson, Active colloids. *Phys. Usp.* **56**, 79 (2013).
9. J. E. Martin, A. Snezhko, Driving self-assembly and emergent dynamics in colloidal suspensions by time-dependent magnetic fields. *Rep. Prog. Phys.* **76**, 126601 (2013).
10. S. Martin, M. Reichert, H. Stark, T. Gisler, Direct observation of hydrodynamic rotation-translation coupling between two colloidal spheres. *Phys. Rev. Lett.* **97**, 248301 (2006).
11. C. Lutz, M. Reichert, H. Stark, C. Bechinger, Surmounting barriers: The benefit of hydrodynamic interactions. *EPL* **74**, 719 (2006).
12. N. Bruot, J. Kotar, F. de Lillo, M. Cosentino Lagomarsino, P. Cicuta, Driving potential and noise level determine the synchronization state of hydrodynamically coupled oscillators. *Phys. Rev. Lett.* **109**, 164103 (2012).
13. H. Nagar, Y. Roichman, Collective excitations of hydrodynamically coupled driven colloidal particles. *Phys. Rev. E* **90**, 042302 (2014).
14. R. Di Leonardo, A. Búzás, L. Kelemen, G. Vizsnyiczai, L. Oroszi, P. Ormos, Hydrodynamic synchronization of light driven microrotors. *Phys. Rev. Lett.* **109**, 034104 (2012).
15. N. Koumakis, R. Di Leonardo, Stochastic hydrodynamic synchronization in rotating energy landscapes. *Phys. Rev. Lett.* **110**, 174103 (2013).
16. E. Lauga, T. R. Powers, Hydrodynamic synchronization of light driven microrotors. *Rep. Prog. Phys.* **72**, 096601 (2009).
17. I. H. Riedel, K. Kruse, J. Howard, A self-organized vortex array of hydrodynamically entrained sperm cells. *Science* **309**, 300–303 (2005).
18. A. Vilfan, F. Jülicher, Hydrodynamic flow patterns and synchronization of beating cilia. *Phys. Rev. Lett.* **96**, 058102 (2006).
19. K. Drescher, K. C. Leptos, I. Tuval, T. Ishikawa, T. J. Pedley, R. E. Goldstein, Dancing *Volvox*: Hydrodynamic bound states of swimming algae. *Phys. Rev. Lett.* **102**, 168101 (2009).
20. E. Lauga, W. R. DiLuzio, G. M. Whitesides, H. A. Stone, Swimming in circles: Motion of bacteria near solid boundaries. *Biophys. J.* **90**, 400–412 (2006).
21. A. P. Berke, L. Turner, H. C. Berg, E. Lauga, Hydrodynamic attraction of swimming microorganisms by surfaces. *Phys. Rev. Lett.* **101**, 038102 (2008).
22. M. B. Wan, C. J. Olson Reichhardt, Z. Nussinov, C. Reichhardt, Rectification of swimming bacteria and self-driven particle systems by arrays of asymmetric barriers. *Phys. Rev. Lett.* **101**, 018102 (2008).
23. R. Di Leonardo, D. Dell'Arciprete, L. Angelani, V. Iebba, Swimming with an image. *Phys. Rev. Lett.* **106**, 038101 (2011).
24. A. Pototsky, A. M. Hahn, H. Stark, Rectification of self-propelled particles by symmetric barriers. *Phys. Rev. E* **87**, 042124 (2013).
25. S. H. Lee, C. M. Liddell, Anisotropic magnetic colloids: A strategy to form complex structures using nonspherical building blocks. *Small* **5**, 1957–1962 (2009).
26. J. Happel, H. Brenner, *Low Reynolds Number Hydrodynamics* (Noordhoff, 1973).
27. F. Martinez-Pedrero, A. Ortiz-Ambriz, I. Pagonabarraga, P. Tierno, Colloidal microworms propelling via a cooperative hydrodynamic conveyor belt. *Phys. Rev. Lett.* **115**, 138301 (2015).
28. P. Lenz, J.-F. Joanny, F. Jülicher, J. Prost, Membranes with rotating motors. *Phys. Rev. Lett.* **91**, 108104 (2003).
29. M. Baron, J. Bławzdziewicz, E. Wajnryb, Hydrodynamic crystals: Collective dynamics of regular arrays of spherical particles in a parallel-wall channel. *Phys. Rev. Lett.* **100**, 174502 (2008).
30. K. Yeo, E. Lushi, P. M. Vlahovska, Collective dynamics in a binary mixture of hydrodynamically coupled microrotors. *Phys. Rev. Lett.* **114**, 188301 (2015).
31. Y. Goto, H. Tanaka, Purely hydrodynamic ordering of rotating disks at a finite Reynolds number. *Nat. Commun.* **6**, 5994 (2015).
32. F. Guzmán-Lastra, A. Keiser, H. Löwen, Fission and fusion scenarios for magnetic microswimmer clusters. *Nat. Commun.* **7**, 13519 (2016).
33. J. R. Blake, A. T. Chwang, Fundamental singularities of viscous flow. *J. Eng. Math.* **8**, 23–29 (1974).
34. J. Elgeti, U. B. Kaupp, G. Gompper, Hydrodynamics of sperm cells near surfaces. *Biophys. J.* **99**, 1018–1026 (2010).
35. M. Driscoll, B. Delmotte, M. Youssef, S. Sacanna, A. Donev, P. Chaikin, Unstable fronts and motile structures formed by microrollers. *Nat. Phys.* **13**, 375–379 (2017).
36. J. J. Erpenbeck, Shear viscosity of the hard-sphere fluid via nonequilibrium molecular dynamics. *Phys. Rev. Lett.* **52**, 1333 (1984).
37. W. Xue, G. S. Grest, Shear-induced alignment of colloidal particles in the presence of a shear flow. *Phys. Rev. Lett.* **64**, 419 (1990).
38. X. Cheng, X. Xu, S. A. Rice, A. R. Dinner, I. Cohen, Assembly of vorticity-aligned hard-sphere colloidal strings in a simple shear flow. *Proc. Natl. Acad. Sci. U.S.A.* **109**, 63–67 (2012).

Acknowledgments

Funding: F.M.-P., A.O.-A., and P.T. acknowledge support from the European Research Council starting grant "DynaMO" (no. 335040). F.M.-P. acknowledges support from the Ramon y Cajal program (RYC-2015-18495). A.O.-A. acknowledges support from the "Juan de la Cierva" program (FJCI-2015-25787). E.N.-A. and I.P. acknowledges support from MINECO (Ministerio de Economía, Industria y Competitividad, Spain), Project FIS2015-67837-P, DURSI Project 2014SGR-922, and Generalitat de Catalunya under Program "ICREA Acadèmia." P.T. acknowledges support from MINECO (FIS2016-78507-C2) and DURSI (2014SGR878). **Author contributions:** F.M.-P. and A.O.-A. performed the experiments. E.N.-A. and I.P. performed the theoretical work. P.T. designed the research and wrote the paper. All authors analyzed the data and discussed the implications of the results. **Competing interests:** The authors declare that they have no competing interests. **Data and materials availability:** All data needed to evaluate the conclusions in the paper are present in the paper and/or the Supplementary Materials. Additional data related to this paper may be requested from the authors.

Submitted 12 September 2017
Accepted 19 December 2017
Published 26 January 2018
10.1126/sciadv.aap9379

Citation: F. Martinez-Pedrero, E. Navarro-Argemí, A. Ortiz-Ambriz, I. Pagonabarraga, P. Tierno, Emergent hydrodynamic bound states between magnetically powered micropropellers. *Sci. Adv.* **4**, eaap9379 (2018).

Science Advances

Emergent hydrodynamic bound states between magnetically powered micropropellers

Fernando Martinez-Pedrero, Eloy Navarro-Argemí, Antonio Ortiz-Ambriz, Ignacio Pagonabarraga and Pietro Tierno

Sci Adv **4** (1), eaap9379.
DOI: 10.1126/sciadv.aap9379